Int J Mater Form (2013) 6:29–40
DOI 10.1007/s12289-011-1062-7

ORIGINAL RESEARCH

Capillary extrusion flow of a fluoropolymer melt

Evan Mitsoulis · Savvas G. Hatzikiriakos

Received: 9 June 2011 / Accepted: 27 July 2011 / Published online: 7 August 2011

Abstract The capillary extrusion-forming flow of a fluoropolymer (FEP) melt was studied both experimentally and numerically. The excess pressure drop due to entry (related to the Bagley correction), the compressibility, and the effect of pressure and temperature on viscosity on the capillary data analysis have been examined. Using a series of capillary dies having different diameters, D, and length-to-diameter L/D ratios, a full rheological characterization has been carried out, and the experimental data have been fitted both with a viscous model (Cross) and a viscoelastic one (the Kaye—Bernstein, Kearsley, Zapas/Papanastasiou, Scriven, Macosko or K-BKZ/PSM model). For the viscous model, the viscosity is a function of both temperature and pressure. For the viscoelastic K-BKZ model, the time-temperature shifting concept has been used for the non-isothermal calculations, while the time-pressure shifting concept has been used to shift the relaxation moduli for the pressure-dependence effect. It was found that the viscous simulations gave good results in the range of apparent shear rates studied. The viscoelastic simulations gave slightly better results in reproducing the experimental data, especially for the entrance pressure losses for $L/D=0$. It is concluded that pressure-dependence of the viscosity and viscoelastic effects are small to moderate in flow of the FEP melt, which is a linear polymer.

E. Mitsoulis (✉)
School of Mining Engineering and Metallurgy,
National Technical University of Athens,
Zografou,
157 80 Athens, Greece
e-mail: mitsouli@metal.ntua.gr

S. G. Hatzikiriakos
Department of Chemical and Biological Engineering,
The University of British Columbia,
Vancouver, BC V6T 1Z4, Canada

Keywords Extrusion forming · Non-isothermal die flow · Fluoropolymers · FEP melt · K-BKZ constitutive equation · Viscoelasticity · Bagley correction

Introduction

Fluoropolymers are among the oldest high-performance polymers, dating from the discovery of polytetrafluoroethylene (PTFE) in 1938 by Dr. Plankett of DuPont. Although their production is small compared to other commodity thermoplastics, such as polyethylene and polypropylene, fluoropolymers are of great commercial and scientific interest due to their unique combination of properties. These include excellent chemical stability and dielectric properties, anti-stick characteristics, mechanical strength, and low flammability [1, 2]. Their most important uses are in electronics and electrical applications, especially for wiring insulation, chemical processing equipment, laboratory ware and tubing, material for roofing and houseware [2, 3].

Fluoropolymers are a class of paraffinic polymers that have some or all of the hydrogen replaced by fluorine. They include polytetrafluoroethylene (PTFE), copolymer of tetrafluoroethylene and hexafluoropropylene (TFE/HFP or FEP), perfluoroalkoxyl resin (PFA), and some others which are discussed in detail by Ebnesajjad [2]. The main focus of this work is on the flow properties of FEP copolymers used in capillary rheometry and extrusion.

Extrusion forming through capillary dies is extensively used in both industry and academia to assess the rheological behaviour of polymer melts at high shear rates before testing their processability in full industrial scale [4]. When such a flow is used and the raw data are collected, a number of important corrections should be applied before the rheological data can be compared with corresponding data from a rotational rheometer [5, 6].

Capillary extrusion flow involves flow through a contraction of a certain angle, where there is a large pressure drop associated with such flow, known as entrance pressure [4–7]. Many studies have previously attempted to examine the origin of entrance pressure and its prediction by some rheological constitutive models. A recent study by the authors gives an extended list of these efforts [8]. The same work studied three different poly-ethylenes, namely a low-density poly-ethylene (LDPE), a linear low-density polyethylene (LLDPE), and a high-density polyethylene (HDPE) in flow through tapered dies. It became apparent that both viscoelasticity *and* pressure-dependence of the viscosity were significant in obtaining high entrance pressures in agreement with experiments. It should be noted that such high entrance pressures are important for other materials as well, such as pastes, as they have been reported by many in the literature [9–12].

Along these lines, it was decided to study this important class of polymers [13, 14] in capillary extrusion. Full experimental capillary data from a large number of capillary dies are analyzed at different temperatures for complete rheological characterization. The collected rheological data are then fitted with appropriate viscous and viscoelastic models for polymer melts, namely the purely viscous Cross model [4] and the viscoelastic K-BKZ model, which has given good predictions of viscoelastic flow phenomena of polymer melts before [4, 8]. The main objective of the study is to predict the entrance pressures and associated Bagley correction (excess pressure losses) in flow of the FEP melt through capillary extrusion-forming dies by appropriate rheological modeling and inclusion of all important effects, such as pressure- and temperature-dependence of viscosity, compressibility and viscous dissipation.

Experimental

FEP is produced by copolymerization of tetrafluoroethylene (TFE) and hexafluoropropylene (HFP). It is mainly a linear polymer (see its structure below). FEP has a crystalline melting point of about 265°C and a density of about 2,150 kg/m^3 at room temperature. Increasing the amount of HFP drops significantly their melting point and thus they become easier to process. It is a soft plastic with tensile strength, wear resistance, and creep resistance lower than those of many other engineering plastics [2].

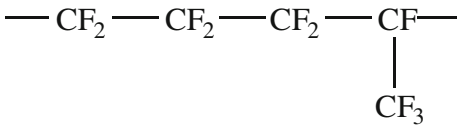

Despite their increasing commercial interest, very few studies have been published on the rheological characterization and processing of these materials [15–18]. This can be partly attributed to the fact that TFE/HFP copolymers (FEP) have a relatively high melting point, and therefore they are difficult to study and process in the melt state.

In the present work, the rheology of an FEP® resin (FEP4100 provided by DuPont) was studied by carrying out experiments in parallel-plate and capillary rheometers. This resin is a tetra-fluoro-ethylene (TFE)—hexa-fluoro-propylene (HFP)—perfluoro(alkyl vinyl ether) (PAVE) copolymer. It has a molecular weight of about 208,000 and a polydispersity index of about 2 [13, 14]. The melting point of this resin is around 260°C, determined by differential scanning calorimetry (DSC) analysis.

First, linear viscoelastic measurements were performed in a Rheometrics System-4 mechanical spectrometer equipped with a parallel-plate fixture (plates of diameter equal to 25 mm). Frequency sweep experiments were performed in a frequency range from 0.01 to 500 rad/s after ensuring that operation was within the linear viscoelastic region (sufficiently small shear strain). Measurements were performed in the temperature range from 300 to 350°C. The lower temperature limit was chosen to avoid residual crystallization, while the upper limit was selected to prevent thermal decomposition. Time-temperature superposition was applied to obtain the master curve (thermo-rheological simplicity) and the data are reported at the selected reference temperature of T_{ref}=300°C.

Capillary experiments were carried out in an Instron constant-speed piston-driven capillary rheometer. Circular extrusion dies of various diameters, D, and length-to-diameter ratios, L/D, were used (Table 1). All the circular dies had a 90°-entrance angle of 2ϕ. Orifice dies (L/D=0) were also used to determine the excess pressure losses (Bagley correction) in order to get an accurate determination of the flow curve. The experiments were carried out at three different temperatures, namely 300°C, 325°C and 350°C. Experimental results for apparent shear rates above about 80 s^{-1} showed severe "melt fracture" (a term used in rheology and polymer processing to signify gross distortions of the extrudate when they are extruded at high enough shear rates [4]) and were not taken into account into

Table 1 Circular dies used (tapered angle 2ϕ=90°, D_{res}=9.525 mm)

Diameter, mm	*L/D* ratios
0.254	0, 20, 40
0.508	0, 20, 40, 100
0.762	0, 10, 20, 40, 70, 100
1.27	0, 20, 40, 70

rheological modeling as they are subject to strong slip phenomena [13, 19, 20].

Governing equations and rheological modelling

We consider the conservation equations of mass, momentum and energy for weakly compressible fluids under non-isothermal, creeping, steady flow conditions. These are written as [21, 22]:

$$\overline{u}\cdot\nabla\rho+\rho(\nabla\cdot\overline{u})=0, \tag{1}$$

$$0=-\nabla p+\nabla\cdot\overline{\overline{\tau}}, \tag{2}$$

$$\rho C_p\overline{u}\cdot\nabla T=k\nabla^2T+\overline{\overline{\tau}}:\nabla\overline{u}, \tag{3}$$

where ρ is the density, $\overline{u}$ is the velocity vector, p is the pressure, $\overline{\overline{\tau}}$ is the extra stress tensor, T is the temperature, C_p is the heat capacity, and k is the thermal conductivity. For a *weakly compressible* fluid, pressure and density are connected as a first approximation through a simple linear thermodynamic equation of state [22]:

$$\rho=\rho_0(1+\beta_c p), \tag{4}$$

where β_c is the isothermal compressibility with the density to be ρ_0 at a reference pressure p_0 (=0).

The viscous stresses are given for inelastic non-Newtonian compressible fluids by the relation [21, 22]:

$$\overline{\overline{\tau}}=\eta(|\dot{\gamma}|)\left(\overline{\overline{\dot{\gamma}}}-\frac{2}{3}(\nabla\cdot\overline{u})\overline{\overline{I}}\right), \tag{5}$$

where $\eta(|\dot{\gamma}|)$ is the apparent non-Newtonian viscosity, which is a function of the magnitude $|\dot{\gamma}|$ of the rate-of-strain tensor $\overline{\overline{\dot{\gamma}}}=\nabla\overline{u}+\nabla\overline{u}^T$, which is given by:

$$|\dot{\gamma}|=\sqrt{\frac{1}{2}\mathrm{II}_{\dot{\gamma}}}=\left(\frac{1}{2}\left(\overline{\overline{\dot{\gamma}}}:\overline{\overline{\dot{\gamma}}}\right)\right)^{1/2}, \tag{6}$$

where $\mathrm{II}_{\dot{\gamma}}$ is the second invariant of $\overline{\overline{\dot{\gamma}}}$

$$\mathrm{II}_{\dot{\gamma}}=\left(\overline{\overline{\dot{\gamma}}}:\overline{\overline{\dot{\gamma}}}\right)=\sum_i\sum_j\dot{\gamma}_{ij}\dot{\gamma}_{ij}, \tag{7}$$

The tensor $\overline{\overline{I}}$ in Eq. (5) is the unit tensor.

To evaluate the role of viscoelasticity in the prediction of Bagley correction, it is instructive to consider first purely viscous models in the simulations. Namely, the Cross model was used to fit the shear viscosity data of the FEP melt. The Cross model is written as [4]:

$$\eta=\frac{\eta_{0,C}}{1+(\lambda\dot{\gamma})^{1-n_C}}, \tag{8}$$

where $\eta_{0,C}$ is the Cross zero-shear-rate viscosity, λ is a time constant, and n_C is the Cross power-law index. The fitted viscosity of the FEP melt by Eq. (8) is plotted in Fig. 1, while the parameters of the model are listed in Table 2. We observe that the FEP melt has a wide Newtonian plateau and then is shear-thinning for shear rates above 1 s^{-1} giving a power-law index n=0.32. The Cross model fits the data well over the range of experimental results.

For easy checks and simple analytical formulas, the high shear-rate range of the viscosity data can be fitted to the power-law model for the viscosity [4]:

$$\eta=K|\dot{\gamma}|^{n-1}, \tag{9}$$

where K is the consistency index and n is the power-law index. These values are also given in Table 2.

For the capillary extrusion flow simulations the effect of pressure on viscosity should be taken into account as this becomes evident below. When flow over long capillaries is considered, the effect of pressure can be moderate. This effect can be taken into account by multiplying the constitutive relation with a pressure-shift factor, a_p, defined by the Barus equation, that is [4–6, 8]:

$$a_p\equiv\frac{\eta}{\eta_{p0}}=\exp(\beta_p p), \tag{10}$$

where η is the viscosity at absolute pressure p, η_{p0} is the viscosity at ambient pressure, and β_p is the pressure coefficient. This coefficient has been reported to be around 10–20 GPa^{-1} for polyethylenes [23, 24]. For the present FEP melt an average value of β_p has been reported to be 30 GPa^{-1} [17].

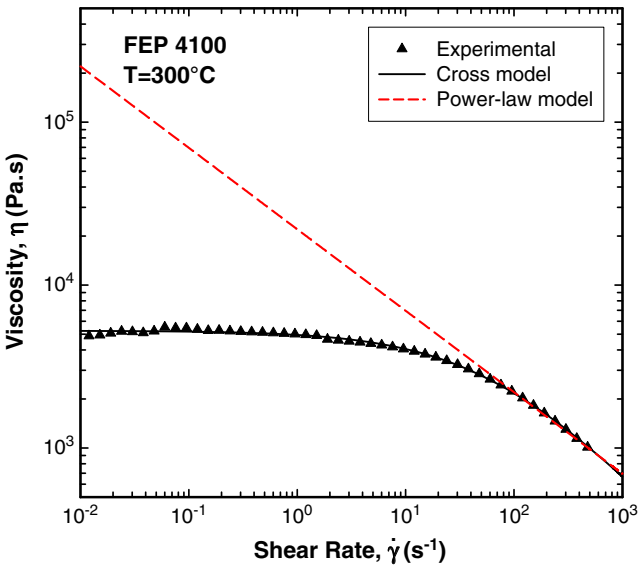

Fig. 1 The shear viscosity of the FEP melt at 300°C fitted with the Cross (Eq. 8) and the power-law (Eq. 9) models using the parameters listed in Table 2

Table 2 Parameters for the FEP melt obeying the Cross model (Eq. 8) and the power-law model (Eq. 9) at 300°C

Parameter	Value
$\eta_{0,C}$	5,246 Pa·s
λ	0.0167 s
n_C	0.316
K	22,000 Pa·s^n
n	0.5

Viscoelasticity is included in the present work via an appropriate rheological model for the stresses. This is a K-BKZ equation proposed by Papanastasiou et al. [25] and modified by Luo and Tanner [26], which has given many good results in predicting viscoelastic flow phenomena associated with polymer melts [21]. This is written as:

$$\tau = \frac{1}{1-\theta}\int_{-\infty}^{t}\sum_{k=1}^{N}\frac{a_k}{\lambda_k}\exp\left(-\frac{t-t'}{\lambda_k}\right) \times \frac{\alpha}{(\alpha-3)+\beta I_{C^{-1}}+(1-\beta)I_C} \times \left[C_t^{-1}(t')+\theta C_t(t')\right]dt', \quad (11)$$

where t is the current time, λ_k and a_k are the relaxation times and relaxation modulus coefficients, N is the number of relaxation modes, α and β are material constants, and I_C, $I_{C^{-1}}$ are the first invariants of the Cauchy-Green tensor $\boldsymbol{C_t}$ and its inverse $\boldsymbol{C_t^{-1}}$, the Finger strain tensor. The material constant θ is given by

$$\frac{N_2}{N_1} = \frac{\theta}{1-\theta}, \quad (12)$$

where N_1 and N_2 are the first and second normal stress differences, respectively. It is noted that θ is not zero for polymer melts, which possess a non-zero second normal stress difference. Its usual range is between 0.1 and 0.2 in accordance with experimental findings [4, 21].

As discussed above, experiments were performed in the parallel-plate and capillary rheometers for the FEP melt to rheologically characterize it. Figure 2 plots the master dynamic moduli G' and G'' for FEP at the reference temperature of 300°C. The model predictions obtained by fitting the experimental data to Eq. (11) with a spectrum of relaxation times, λ_k, and coefficients, a_k, determined by a non-linear regression package [27], are also plotted. The parameter α is found by fitting the experimental shear viscosity data [27]. The parameter β is found by fitting experimental elongational viscosity data [27]. For a linear polymer, like FEP or HDPE [28], these data follow the Linear Viscoelastic Envelope (LVE) [4] in start-up extensional experiments; they are not shown here due to the well known strain-thinning behaviour of linear polymers in extension [4]. The parameters found from the fitting

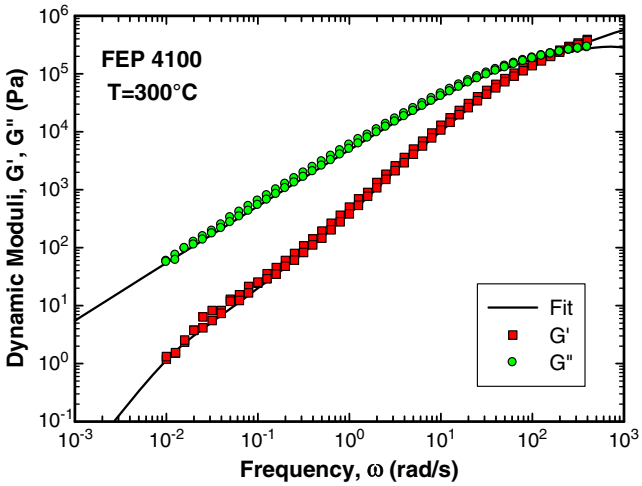

Fig. 2 Experimental data (*symbols*) and model predictions of storage (G') and loss (G'') moduli for the FEP melt at 300°C using the relaxation times listed in Table 3

procedure are listed in Table 3. The relaxation spectrum is used to find the average relaxation time, $\overline{\lambda}$, and zero-shear-rate viscosity, η, according to the formulas (Table 3):

$$\overline{\lambda} = \frac{\sum_{k=1}^{N} a_k\lambda_k^2}{\sum_{k=1}^{N} a_k\lambda_k}, \quad (13)$$

$$\eta_0 = \sum_{k=1}^{N} a_k\lambda_k. \quad (14)$$

The values of these parameters are $\overline{\lambda}$=2.6 s, η_0= 5482 Pa·s, indicating a slightly elastic melt with a rather small average relaxation time, certainly less elastic than the PE melts studied before [8].

Figure 3 plots a number of calculated and experimental material functions for the FEP melt at the reference temperature of 300°C. Namely, data for the shear viscosity, η_S, the elongational viscosity, η_E, and the first normal stress

Table 3 Relaxation spectrum and material constants for the FEP melt obeying the K-BKZ model (Eq. 11) at 300°C (α=7.17, β = 0.6, θ= −0.111, $\overline{\lambda}$=2.6 s, η_0=5,482 Pa·s)

k	λ_k (s)	a_k (Pa)
1	0.1147×10^{-2}	0.49050×10^{6}
2	0.6039×10^{-2}	0.22702×10^{6}
3	0.2940×10^{-1}	66,224
4	0.1911	4823.1
5	1.66	172.41
6	10.13	18.628
7	56.520	3.6235

Table 4 Values of the various parameters for the FEP melt at 300°C

Parameter	Value	Reference
β_c	0.00095 MPa^{-1}	[36]
β_p	0.03 MPa^{-1}	[17]
m	$1.39\times10^{-4}\ Pa^{n_p-1}$	This work
n_p	0.54	This work
ρ	1.492 g/cm^3	[35]
C_p	0.96 J/(g K)	[34]
k	0.00255 J/(s cm K)	[34]
E	50,000 J/mol	[14]
R_g	8.3143 J/(mol K)	[4]
T_0	300°C (573 K)	[14]

difference, N_1, are plotted as functions of corresponding rates (shear or extensional).

Non-isothermal modeling

The viscoelastic stresses calculated by the above constitutive equation (Eq. 11) enter in the energy equation (Eq. 4) as a contribution to the viscous dissipation term. This assumes that all the elastic stored energy in the material is converted into heat and serves to raise the temperature of the melt. This treatment has been the standard practice in non-isothermal simulations so far (see, e.g., [29–32]) and it is followed in the present work as well. Peters and Baaijens [33] have devised a different approach to handle the splitting between the viscous contribution to energy dissipation and elastic stored energy. However, such a development is beyond the scope of this study.

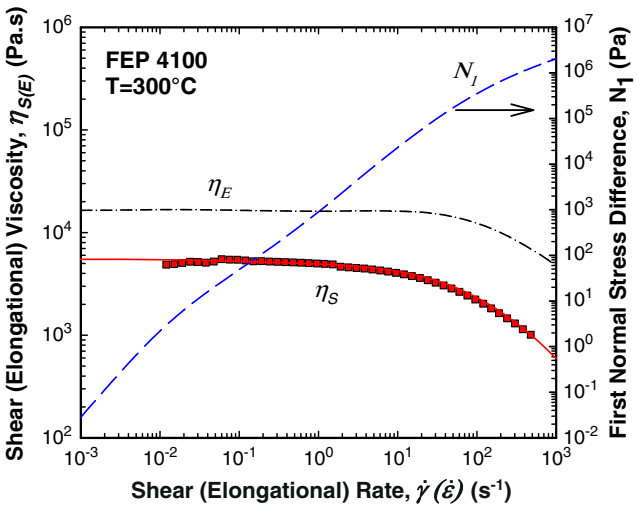

Fig. 3 Experimental data (*solid symbols*) and model predictions of shear viscosity, η_S, first normal stress difference, N_1, and elongational viscosity, η_E, for the FEP melt at 300°C using the K-BKZ model (Eq. 11) with the parameters listed in Table 3

The details of the non-isothermal modeling are given in earlier publications [29–33] and will not be repeated here. Suffice it to say that they involve the Arrhenius temperature-shifting function, a_T, given by [4, 29]:

$$a_T(T) = \frac{\eta}{\eta_0} = \exp\left[\frac{E}{R_g}\left(\frac{1}{T} - \frac{1}{T_0}\right)\right]. \tag{15}$$

In the above, η_0 is a reference viscosity at T_0, E is the activation flow energy, R_g is the ideal gas constant, and T_0 is a reference temperature (in K). The activation energy can be calculated from the shift factors determined by applying the time-temperature superposition to obtain the master curves plotted in Fig. 2 [4, 14]. It was found to be 50,000 J/mol.

In the present work we have applied the above equation to derive the non-isothermal constitutive equation from the isothermal one. This method is based on the time-temperature superposition principle and simply consists of shifting the relaxation times λ_k from the temperature history within the material's internal time scale t' [30]. The equation used to shift the relaxation times in the material's history is given by [30, 31]:

$$\lambda_k(T'(t')) = \lambda_k(T_0)a_T(T'(t')). \tag{16}$$

where T' is the temperature at time t'.

The viscoelastic stresses calculated by the non-isothermal version of the above constitutive equation (Eq. 11) enter in the energy equation (Eq. 3) as a contribution to the viscous dissipation term.

The thermal properties of the melt have been gathered from various sources. The thermal conductivity was given in the textbook by Van Krevelen [34] to be 0.255 W/m·K, and the heat capacity was 0.96 in kJ/(kg K) at 300°C [34]. The density was 2.12–2.17 g/cm^3 at room temperature [34], while at 300°C, its value was 1.492 g/cm^3 [35].

All these properties and their provenance are listed together in Table 4. In this table, we have also added a typical value for polymer melts for the coefficient of compressibility, β_c, from Hatzikiriakos and Dealy [36].

The various thermal and flow parameters are combined to give appropriate dimensionless numbers [37, 38]. The relevant ones here are the Peclet number, Pe, and the Nahme-Griffith number, Na. These are defined as:

$$Pe = \frac{\rho C_p U R}{k}, \tag{19}$$

$$Na = \frac{\overline{\eta} E U^2}{k R_g T_0^2}, \tag{20}$$

where $\overline{\eta} = f(U/R)$ is a nominal viscosity given by the Cross model (Eq. 8) at a nominal shear rate of U/R, and U

$(= \dot{\gamma}_A R/4)$ is the average velocity in the capillary die. The *Pe* number represents the ratio of heat convection to conduction, and the *Na* number represents the ratio of viscous dissipation to conduction and indicates the extent of coupling between the momentum and energy equations. A thorough discussion of these effects in non-isothermal polymer melt flow is given by Winter [37].

With the above properties and a die radius R=0.04 cm, the dimensionless thermal numbers are in the ranges: $3.2<Pe<32$, $0.001<Na<0.048$, showing a moderate convection ($Pe>1$), and a very small coupling between momentum and energy equations ($Na<0.1$). A value of $Na>1$ indicates temperature non-uniformities generated by viscous dissipation, and a strong coupling between momentum and energy equations, which may be true for polyethylene melts [38], but not for the FEP melt at hand. More details are given in Table 5.

The fully developed values for temperature occur for $L/D=\infty$ and give a maximum temperature rise ΔT_{max} at the centreline of the tube according to the formula for a power-law fluid [39]:

$$\Delta T_{max} = \frac{K}{k}\left(\frac{nR}{3n+1}\right)^2\left[\left(\frac{n+1}{n}\right)\frac{V_{max}}{R}\right]^{n+1}. \quad (21)$$

According to Eq. (21) and for R=0.04 cm, we get a ΔT_{max}=1.4°C. Thus, a small temperature rise is expected for very long dies, but for shorter dies as the ones used here, the non-isothermal simulations are not necessary.

Pressure-dependent modeling

Similarly with the time-temperature superposition principle where the stresses are calculated at a different temperature using the shift factor a_T, the time-pressure superposition principle can be used to account for the pressure effect on the stresses. In both cases of viscous or viscoelastic models, the new stresses are calculated using the pressure-shift factor a_p. For viscous models, Eq. (10) is used to modify the viscosity. For viscoelastic models, such as the K-BKZ model (Eq. 11), the pressure-shift factor modifies the relaxation moduli, a_k, according to:

$$a_k(p(t')) = a_k(p_0)a_p(p(t')). \quad (22)$$

This is equivalent to multiplying the stresses by a_p, according to Eq. (11). It should be noted that a_p is an exponential function of β_p.

The pressure-dependence of the viscosity gives rise to the dimensionless pressure-shift parameter, B_p. This is defined as:

$$B_p = \frac{\beta_p \overline{\eta} U}{R}. \quad (23)$$

Similarly, the compressibility coefficient β_c gives rise to the dimensionless compressibility parameter, B_c. This is defined as:

$$B_c = \frac{\beta_c \overline{\eta} U}{R}. \quad (24)$$

When B_p=0, we have no pressure-dependence of the viscosity, and when B_c=0, we have incompressible flow. For the present data, we get: $5.4\times10^{-4}<B_p<3.5\times10^{-3}$ and $1.7\times10^{-5}<B_c<1.1\times10^{-4}$, showing a moderate dependence of viscosity on pressure and an even weaker compressibility effect in the range of simulations. More details are given in Table 5.

Table 5 Range of the dimensionless parameters in the flow of FEP melt at 300°C (die radius R=0.04 cm)

Apparent Shear Rate, $\dot{\gamma}_A$ (s^{-1})	Peclet Number, *Pe*	Nahme Number, *Na*	Compressibility Parameter, B_c	Pressure-Shift Parameter, B_p
6	3.2	0.001	1.7×10^{-5}	5.36×10^{-4}
9	4.8	0.002	2.44×10^{-5}	7.71×10^{-4}
15	8.0	0.004	3.8×10^{-5}	1.2×10^{-3}
30	16.1	0.014	6.69×10^{-5}	2.1×10^{-3}
60	32.1	0.048	1.12×10^{-4}	3.5×10^{-3}

Method of solution

The solution of the above conservation and constitutive equations is carried out with two codes, one for viscous flows (*u-v-p-T-h* formulation) [40] and one for viscoelastic flows [32, 41]. The formulation *u-v-p-T-h* refers to the primary variables, i.e., the two velocities u and v, the pressure p, the temperature T, and the free surface h (which is not used here). Quadratic interpolation functions are used for all variables except the pressure for which linear interpolation functions are used. For the temperature T, a subdivision of the quadratic parent element into 4 bilinear quadrilateral elements is also used for implementing the Streamline-Upwind/Petrov-Galerkin (SU/PG) scheme [38, 40], which stabilizes the T-solution in flows dominated by convection (high Peclet number flows). However, due to the mild conditions studied here, the results were identical with or without SU/PG.

The boundary conditions (BC) for the problem at hand are well known and can be found in our earlier publication [32]. Briefly, we assume no-slip and a constant temperature T_0 at the solid walls; at entry, a fully-developed velocity profile is imposed, corresponding to the flow rate at hand and a constant temperature T_0 is assumed; at the outlet, zero

surface traction and zero heat flux are assumed; at the centerline, symmetry is assumed.

The viscous simulations are extremely fast and are used as a first step to study the whole range of parameter values and die designs. The viscoelastic simulations admittedly are harder to do and they need good initial flow fields to get solutions at elevated apparent shear rates. In our recent work [8], we explained how it was possible for the first time to do viscoelastic computations up to very high apparent shear rates (1000 s^{-1}) with good results. Briefly, the solution strategy starts at a given apparent shear rate from the viscous non-isothermal solution without pressure dependence, and then using this as an initial solution it continues for the non-isothermal viscoelastic solution with all effects present. The results for L/D=0 were obtained as in Ref. [8] by subtracting from the longest dies (L/D=100) results obtained for the same dies without the reservoir. Thus, it was found again necessary to use a long die to fully unravel the viscoelastic stresses of the FEP melt.

Experimental results

Figure 4 shows the apparent flow curves for resin FEP® 4100 obtained with dies having a constant diameter (D= 0.762 mm) and various L/D ratios. It can be seen that the data do not fall on a single curve. Instead, the apparent flow curves shift to higher values of the wall shear stress with increasing L/D ratio, thus pressure. This implies that the viscosity of FEP® 4100 is a function of pressure, usually taken as the Barus equation (Eq. 10).

To obtain the pressure coefficient of viscosity, β_p, the data points corresponding to various values of L/D ratio in the smooth region were brought together on a single curve by varying β_p. It is noted that at very low shear rates and

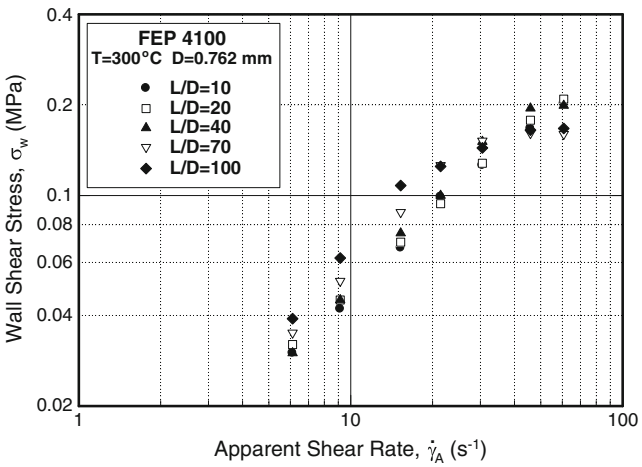

Fig. 4 Flow curves for the capillary extrusion of the FEP melt at 300°C determined with dies having L/D ratios from 10 to 100

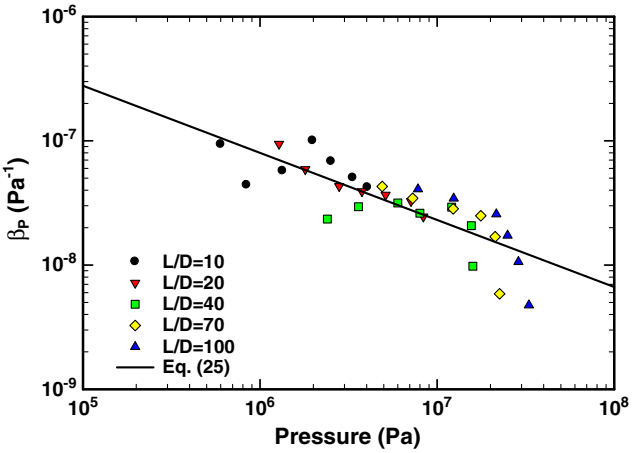

Fig. 5 The pressure coefficient, β_p, as a function of pressure

for small L/D ratio, the wall shear stress slightly depends on pressure and this dependence increases with an increase of L/D and shear rate. In our case, the various β_p coefficients determined by using data from various dies having different L/D (variation of pressure at a given shear rate) exhibit a power-law dependency on pressure as can be seen from Fig. 5. This dependence can be expressed by the following equation:

$$\beta_p = mp^{-n_p}, \tag{25}$$

where $m=1.39\times10^{-4}$ Pa^{n_p-1} and n_p=0.54, with the pressure p given in Pa. The pressure-corrected flow data for the FEP are plotted in Fig. 6. Essentially the shear stress data plotted in Fig. 4 were divided by $\exp(\beta_p p)$, where p is the average pressure along the capillary estimated as $(2L/D)_w$. It can be observed that a relatively good superposition of the data results. There are outliers for the longer dies with L/D=70 and 100, and these data have not been taken into

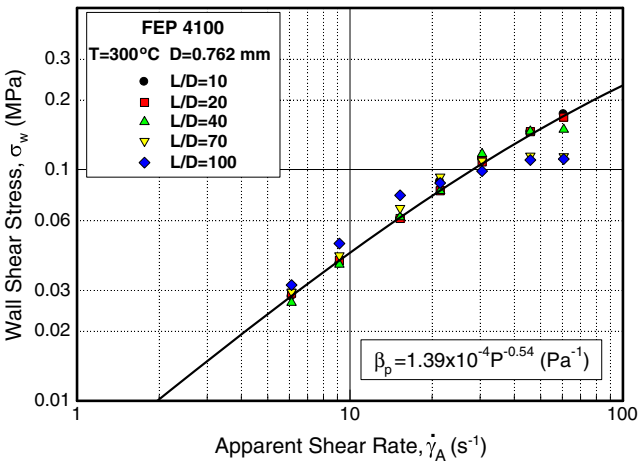

Fig. 6 The pressure-corrected flow curves for the capillary extrusion of the FEP melt at 300°C determined with dies having L/D ratios from 10 to 100

account as they may refer to data where "melt fracture" (or gross distortion of the extrudate when extruded at high enough shear rates) has started occurring [17]. The values of β_p plotted in Fig. 5 agree well with the reported values in the literature [23, 24].

Figure 7 plots the end pressure (Bagley correction) of the FEP melt at 300°C obtained with capillary dies having lengths of L/D=0 and different diameters, D. These data will be simulated using the models discussed above.

Numerical results

Viscous modeling

It is instructive to perform first calculations with a purely viscous model, so that the effect of viscoelasticity will become evident later. The numerical simulations have been undertaken using the purely viscous Cross model (Eq. 8). This constitutive relation is solved together with the conservation equations of mass and momentum either for an incompressible or compressible fluid under isothermal or non-isothermal conditions (conservation of energy equation) without or with the effect of pressure-dependence of the viscosity.

For the finite element mesh arrangement we have used our experience with viscous and viscoelastic flows and chosen a grid that progressively adds more elements as one moves towards the singularity at the entrance to the die, while the elements become bigger as one moves away from the singularity. A typical finite element grid is shown in Fig. 8 for L/R=20. The domain represents a 12.5:1 abrupt circular contraction with an entrance angle 2ϕ = 90°. The grid consists of 1700 elements, 7161 nodes, and 22,261 unknown degrees of freedom (d.o.f.), while a 4-times

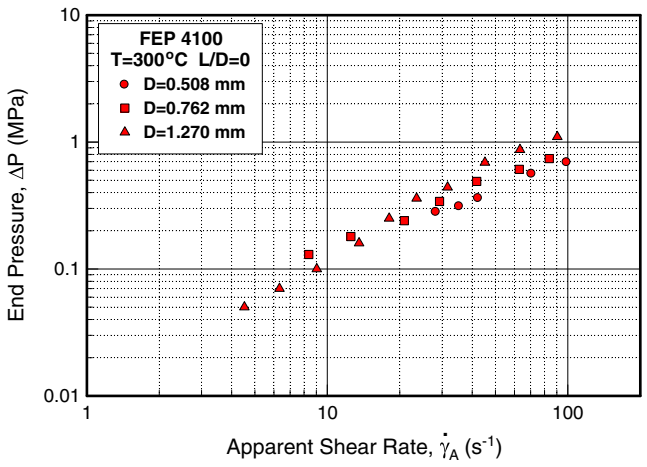

Fig. 7 The end pressure (Bagley correction) of the FEP melt at 300°C for different diameters D

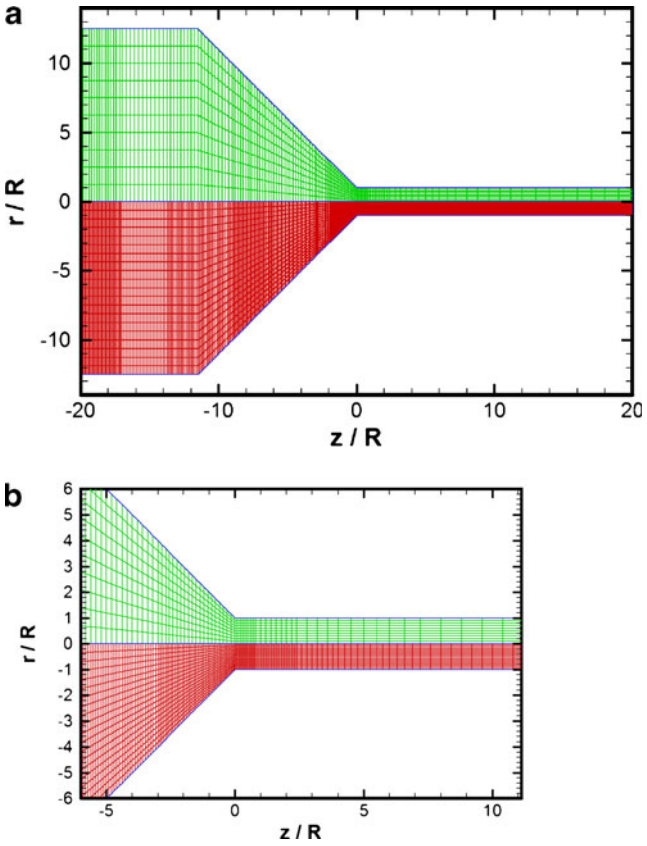

Fig. 8 **a** A typical finite element grid for the simulations in an 12.5:1 tapered circular contraction with L/R=20 and 2ϕ=90°. The upper grid (M1) consists of 1700 elements and 7161 nodes, while the lower grid is created by subdivision of each M1 element into 4 sub-elements to form a denser grid for checking the results for grid-independence; **b** detailed grids near the die entry

denser grid is also used, having been created by subdivision of each element into 4 sub-elements for checking purposes of grid-independent results. This checking consists of reporting the overall pressures in the system from the two meshes and making sure that the differences are less than 1% between the two results. Having fixed the Cross model parameters and the problem geometry, the only parameter left to vary was the apparent shear rate in the die ($\dot{\gamma}_A = 4Q/\pi R^3$). Simulations were performed for the stable range of experimental apparent shear rates, namely from 5 s^{-1} to 60 s^{-1}, before melt fracture sets in. We have chosen for detailed studies a die with D=0.762 mm having a constant contraction ratio D_{res}/D=12.5 but different lengths.

First, runs were carried out to study each effect separately, namely: (a) the effect of compressibility alone, (b) the effect of a pressure-dependent viscosity alone, (c) the effect of a temperature-dependent viscosity alone, and these were compared with the *base case* of no effects at all ($\beta_c=\beta_p=a_T=0$).

It was found that compressibility played a negligible role, as the results were virtually the same with or without

compressibility and they are not shown here. Admittedly, this is expected because the value for FEP of β_c= 0.00095 MPa^{-1} is small, giving rise to very small values for the dimensionless compressibility parameter B_c in Table 5 in the range of simulations. The same was true for the LDPE and HDPE melts in our previous work [8].

The effect of temperature-dependent viscosity was also very small in the range of simulations (not shown here) never exceeding a maximum temperature rise of a fraction of a degree. This is not surprising given the very low *Na* numbers of Table 5.

On the other hand, a pressure-dependence of the viscosity, with a variable value of β_p obeying Eq. (25) plays a considerable role (Fig. 9 with all effects present) augmenting the pressure drop by about 16% at the highest apparent shear rate. The pressure is higher than the base case for all apparent shear rates, due to the dominant effect of pressure-dependence of the viscosity. This effect is the most significant and masks out the other two negligible contributions of compressibility and temperature-dependence of viscosity.

When the die is longer (L/D=40), the overall effects are more pronounced as evidenced in Fig. 10. At the highest shear rates we see a curvature in the pressure drop in the die due to the pressure-dependence of the viscosity.

Collecting all the pressure results together for the four dies with L/D=0.2, 10, 20, 40, and five apparent shear rates

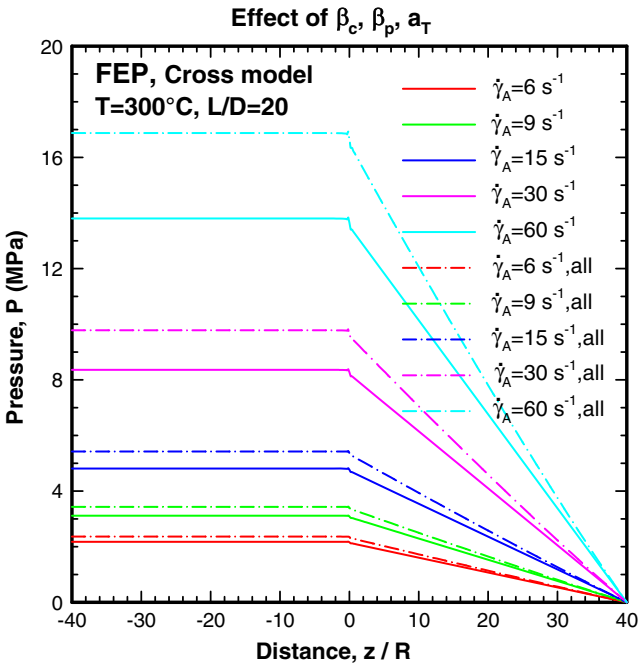

Fig. 9 The effects of compressibility, and pressure- and temperature-dependent viscosity, all taken together, on the pressure distribution for the FEP melt at 300°C at various values of apparent shear rate. Solid lines are for the base case (β_c=β_p=a_T=0). The dominant effect is the pressure-dependence of the viscosity

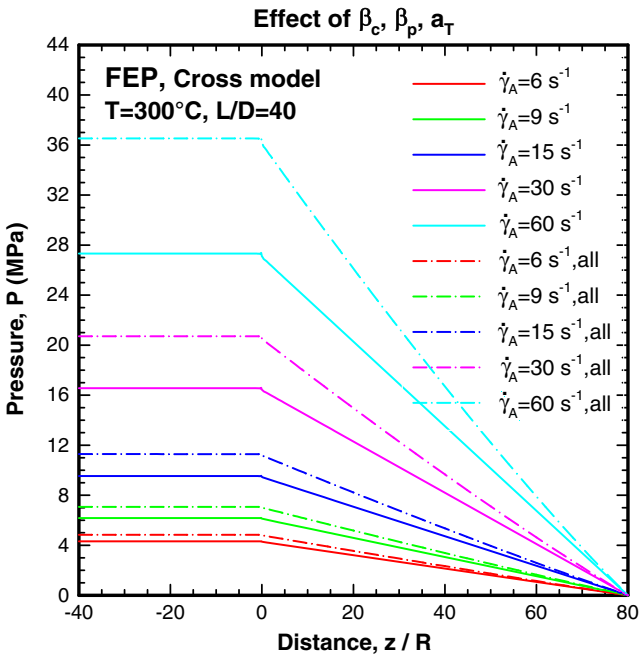

Fig. 10 The effects of compressibility, and pressure- and temperature-dependent viscosity, all taken together, on the pressure distribution for the FEP melt at 300°C at various values of apparent shear rate but for a longer die (L/D=40). Solid lines are for the base case (β_c=β_p=a_T=0). The dominant effect is the pressure-dependence of the viscosity

$\dot{\gamma}_A$ gives the well known Bagley plot shown in Fig. 11. The experimental results are shown as symbols while the numerical results here and in the subsequent graphs are shown as lines. These simulation results have been obtained with all parameters switched on, i.e., compressibility, pressure- and temperature-dependence of viscosity. The results agree well with the experimental data, except for the well-known inability of a viscous model to capture the end correction (for L/D=0). A purely viscous model for FEP predicts end corrections lower than the experimental ones. It is then at this point that we turn our attention to the viscoelastic results.

Viscoelastic modeling

It is again instructive to compare pressure distributions between the viscous and the viscoelastic models with all effects present. This is done in Fig. 12, where we show the pressure results from the Cross and the K-BKZ models for the case of L/D=40 with D=0.762 mm. The viscoelastic pressures are higher than the viscous ones, and this becomes more apparent at elevated shear rates (maximum difference of 6% at 60 s^{-1}). However, it seems that the overall pressure results are well captured by both models mainly due to the small range of apparent shear rates studied, in relation to the intersection point of G' and G" of Fig. 2.

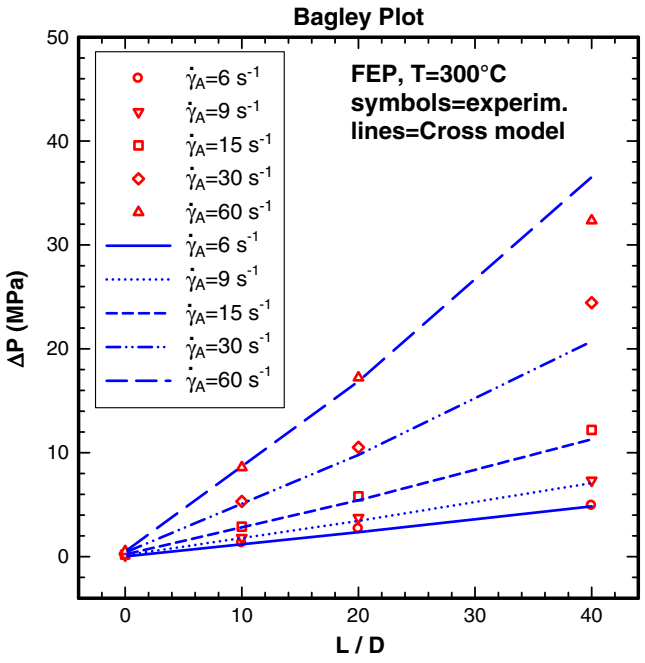

Fig. 11 The effect of *L/D* on the pressure for the FEP melt at 300°C at various values of apparent shear rate (all effects accounted for). Simulations with the purely viscous Cross model (Eq. 8)

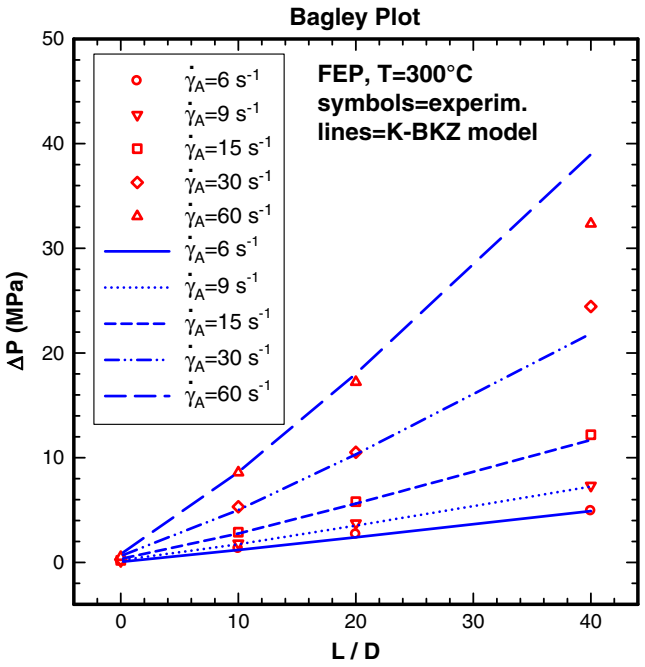

Fig. 13 The effect of *L/D* on the pressure for the FEP melt at 300°C at various values of apparent shear rate (all effects accounted for). Simulations with the K-BKZ model (Eq. 11)

Collecting again all the pressure results together for the four dies with *L/D*=0.2, 10, 20, 40 and five apparent shear rates $\dot{\gamma}_A$ gives the corresponding viscoelastic Bagley plot shown in Fig. 13. The agreement is again good as with the viscous simulations, but the more severe test is the Bagley correction for *L/D*=0. This is shown in Fig. 14. We see that the viscoelastic simulations better capture the experimental results, which are underestimated by the viscous simulations.

The small effect of different die diameters *D* on the end correction was not captured by the model as such. Such experimental data, where the entry pressure has shown a diameter dependence, have been reported by Meissner [42]. At this point the origin of this dependence is not known and it is a subject of further investigation.

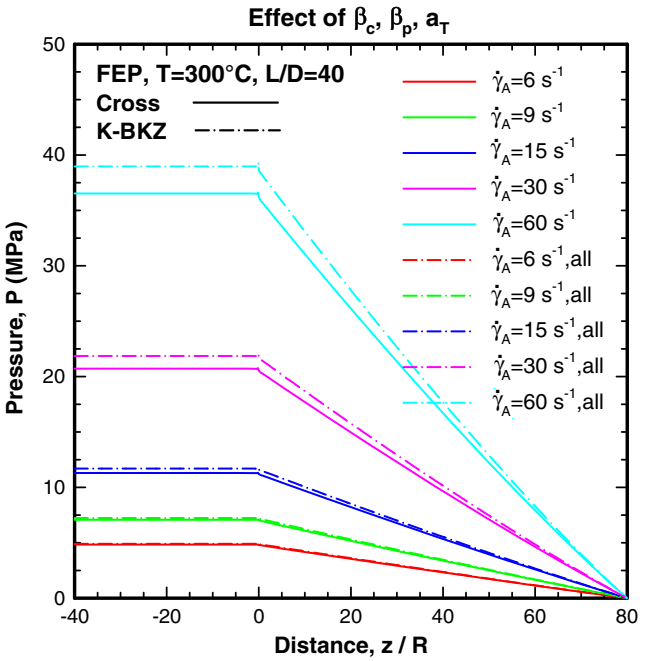

Fig. 12 Viscous vs. viscoelastic results for the axial pressure distribution with all effects present for the FEP melt at 300°C at various values of apparent shear rate (*L/D*=40)

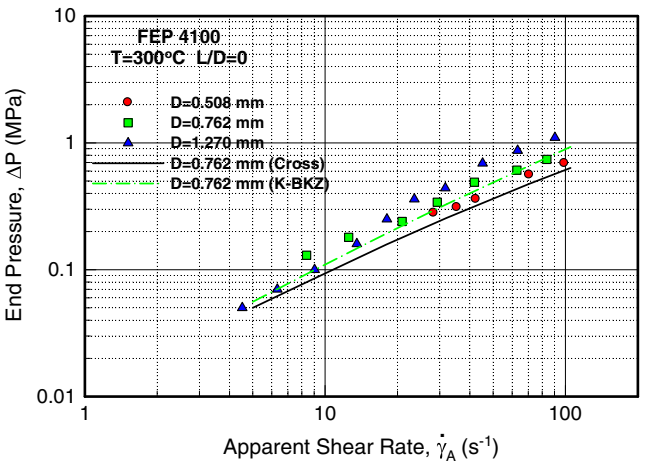

Fig. 14 The end pressure (Bagley correction) of the FEP melt at 300°C for different diameters *D*. Symbols are experimental data, lines are simulation results with the Cross and the K-BKZ models

Conclusions

A FEP melt has been studied in entry flows through capillary dies with different *L/D* ratios with the purpose of predicting the entry pressure to capillaries (Bagley correction) and its flow behaviour in pressure-driven circular extrusion-forming flows. Full rheological characterization was carried out both with a viscous (Cross) and a viscoelastic (K-BKZ) model. All necessary material properties data were collected for the simulations.

The viscous model was found to predict well the extrusion pressures but underestimated the Bagley correction (*L/D*=0). On the other hand, the viscoelastic model showed a slight but still better agreement with the experimental results. The simulations showed that: (a) compressibility is not important in these steady flows; (b) viscous dissipation is negligible, even for the more severe conditions (high *L/D* and apparent shear rates); (c) the pressure-dependence of viscosity is moderate and must be accounted for, especially for the more severe conditions (high *L/D* and apparent shear rates). This is the first time that all these effects are taken into account in a viscoelastic simulation for a fluoropolymer melt.

Acknowledgements Financial assistance from the Natural Sciences and Engineering Research Council (NSERC) of Canada and the programme "PEBE 2009-2011" for basic research from NTUA are gratefully acknowledged.

References

1. Imbalzano AE, Kerbow DL (1994) Advances in fluoroplastics. Trends Pol Sci 2:26–30
2. Ebnesajjad S (2003) Melt Processible Fluoropolymers. Elsevier, New York
3. Domininghaus H (1993) Plastics for Engineers: Materials, Properties, Applications, Hanser, Munich
4. Dealy JM, Wissbrun KF (1990) Melt Rheology and its Role in Plastics Processing—Theory and Applications. Van Nostrand Reinhold, New York
5. Laun HM (2003) Pressure dependent viscosity and dissipative heating in capillary rheometry of polymer melts. Rheol Acta 42:295–308
6. Laun HM (2004) Capillary rheometry for polymer melts revisited. Rheol Acta 43:509–528
7. Bagley EB (1957) End corrections in the capillary flow of polyethylene. J Appl Phys 28:193–209
8. Ansari M, Alabbas A, Mitsoulis E, Hatzikiriakos SG (2010) Entry flow of polyethylene melts in tapered dies. Intern Polym Proc 25:287–296
9. Horrobin DJ, Nedderman RM (1998) Die entry pressure drops in paste extrusion. Chem Eng Sci 53:3215–3225
10. Gibson AG (1998) Converging Dies. In: Collyer AA, Gregg DW (eds) Rheological Measurements. Chapman and Hall, London
11. Ariawan AB, Ebnesajjad S, Hatzikiriakos SG (2002) Paste extrusion of polytetrafluoroethylene (PTFE) fine powder resins. Can J Chem Eng 80:1153–1165
12. Ochoa I, Hatzikiriakos SG (2005) Paste extrusion of PTFE: viscosity and surface tension effects. Powder Technology 153:108–118
13. Rosenbaum E, Hatzikiriakos SG, Stewart CW (1995) Flow implications in the processing of teflon® resins. Intern Polym Proc 10:204–212
14. Rosenbaum E, Hatzikiriakos SG, Stewart CW (1998) Rheological characterization of well defined TFE/HFP copolymers. Rheol Acta 37:279–288
15. Tordella JP (1963) An unusual mechanism of extrusion of polytetrafluoroethylene at high temperature and pressure. J Appl Polym Sci 7:215–229
16. Tordella JP (1969) Unstable flow of molten polymers, in rheology. Theory and Application 5:57–92
17. Rosenbaum EE (1998) Rheology and processability of FEP Teflon resins for wire coating, PhD thesis, University of British Columbia, Vancouver, Canada
18. Rosenbaum EE, Randa S, Hatzikiriakos SG, Stewart CW (2000) Boron nitride as a processing aid for the extrusion of polyolefins and fluoropolymers. Polym Eng Sci 40:179–190
19. Hatzikiriakos SG, Dealy JM (1991) Wall slip of molten high density polyethylene I. Sliding plate rheometer studies. J Rheol 35:497–523
20. Hatzikiriakos SG, Dealy JM (1992) Wall slip of molten high density polyethylene. II. Capillary rheometer studies. J Rheol 36:703–741
21. Tanner RI (2000) Engineering Rheology, 2nd edn. Oxford University Press, Oxford
22. Mitsoulis E, Hatzikiriakos SG (2009) Steady flow simulations of compressible PTFE paste extrusion under severe wall slip. J Non-Newtonian Fluid Mech 157:26–33
23. Sedlacek T, Zatloukal M, Filip P, Boltizar A, Saha P (2004) On the effect of pressure on the shear and elongational viscosities of polymer melts. Polym Eng Sci 44:1328–1337
24. Carreras ES, El Kissi N, Piau J-M, Toussaint F, Nigen S (2006) Pressure effects on viscosity and flow stability of polyethylene melts during extrusion. Rheol Acta 45:209–222
25. Papanastasiou AC, Scriven LE, Macosko CW (1983) An integral constitutive equation for mixed flows: viscoelastic characterization. J Rheol 27:387–410
26. Luo X-L, Tanner RI (1988) Finite element simulation of long and short circular die extrusion experiments using integral models. Int J Num Meth Eng 25:9–22
27. Kajiwara T, Barakos G, Mitsoulis E (1995) Rheological characterization of polymer solutions and melts with an integral constitutive equation. Int J Polymer Analysis & Characterization 1:201–215
28. Luo X-L, Mitsoulis E (1990) A numerical study of the effect of elongational viscosity on vortex growth in contraction flows of polyethylene melts. J Rheol 34:309–342
29. Luo X-L, Tanner RI (1987) A pseudo-time integral method for non-isothermal viscoelastic flows and its application to extrusion simulation. Rheol Acta 26:499–507
30. Alaie SM, Papanastasiou TC (1993) Modeling of non-isothermal film blowing with integral constitutive equations. Intern Polym Proc 8:51–65
31. Beaulne M, Mitsoulis E (2007) Effect of viscoelasticity in the film-blowing process. J Appl Polym Sci 105:2098–2112
32. Barakos G, Mitsoulis E (1996) Non-isothermal viscoelastic simulations of extrusion through dies and prediction of the bending phenomenon. j non-Newtonian Fluid Mech 62:55–79
33. Peters GWM, Baaijens FPT (1997) Modelling of non-isothermal viscoelastic flows. J Non-Newtonian Fluid Mech 68:205–224
34. Van Krevelen DW (1990) Properties of Polymers, 3rd edn. Elsevier, New York
35. Ebnesajjad S (2000) Fluoroplastics: Vol. 2, Melt Processing Fluoroplastics. William Andrew Inc, New York

36. Hatzikiriakos SG, Dealy JM (1994) Start-up pressure transients in a capillary rheometer. Polym Eng Sci 34:493–499
37. Winter HH (1977) Viscous dissipation in shear flows of molten polymers. Adv Heat Transfer 13:205–267
38. Mitsoulis E, Wagner R, Heng FL (1988) Numerical simulation of wire-coating low-density polyethylene: theory and experiments. Polym Eng Sci 28:291–310
39. Bird RB, Armstrong RC, Hassager O (1987) Dynamics of polymeric liquids, vol. 1: Fluid mechanics, 2nd Ed. Wiley, New York
40. Hannachi A, Mitsoulis E (1993) Sheet coextrusion of polymer solutions and melts: comparison between simulation and experiments. Adv Polym Technol 12:217–231
41. Luo X-L, Mitsoulis E (1990) An efficient algorithm for strain history tracking in finite element computations of non-Newtonian fluids with integral constitutive equations. Int J Num Meth Fluids 11:1015–1031
42. Meissner J (1975) Basic parameters, melt rheology, processing and end-use properties of three similar low density polyethylene samples. Pure Appl Chem 42:551–612